ISSN 1063-7834, Physics of the Solid State, 2013, Vol. 55, No. 5, pp. 960–965. © Pleiades Publishing, Ltd., 2013.
Original Russian Text © A.D. Gorlov, 2013, published in Fizika Tverdogo Tela, 2013, Vol. 55, No. 5, pp. 883–887.

DIELECTRICS

Hyperfine Structure of EPR Spectra of Gd^{3+} Odd Isotopes in $PbMoO_4$, $Pb_5Ge_3O_{11}$, YVO_4, and Quadrupole Interaction (Temperature Dependence)

A. D. Gorlov

Institute of Physics and Applied Mathematics, Ural Federal University named after the First President of Russia B.N. Yeltsin (Ural State Technical University–UPI), pr. Lenina 51, Yekaterinburg, 620083 Russia

e-mail: Anatoliy.Gorlov@usu.ru

Received August 20, 2012

Abstract—A hyperfine structure of EPR signals of odd isotopes Gd^{3+} in $Pb_5Ge_3O_{11}$, $PbMoO_4$, and YVO_4 single crystals has been investigated at different temperatures. The observation of forbidden (with the nuclear spin flip) transitions has made it possible to determine quadrupole interaction P_2^0 associated with the gradient of the electric field of ligands at the impurity. It has been shown for the first time that, under the condition $|P_2^0| \geq |A_{x,y}|$ (A_i are the tensor components), not only the magnitudes of splitting but also the observed asymmetry in a hyperfine structure (in perpendicular orientations of the magnetic field) depends on mutual signs of parameters of initial splitting b_2^0 and P_2^0. Results of studying the spectra have demonstrated that $|b_2^0(T)|/|P_2^0(T)|$ ~ const for a concrete single crystal, which assumes the similarity of physical mechanisms determining these parameters.

DOI: 10.1134/S1063783413050119

1. INTRODUCTION

Investigation of the hyperfine structure (HFS) of EPR signals of impurity centers (ICs) has been performed from the time of discovery of the electron paramagnetic resonance. However, it turned out that there are not completely studied features of the HFS in the situation with the magnitude of the quadrupole interaction (QI) $|P_2^0| \geq |A_i|$ ($i = x, y$) of components of intrinsic hyperfine interaction (HFI) for $S > 1/2$ and $I > 1/2$. Our investigations of the HFS of EPR transitions for odd isotopes Gd^{3+} ($S = 7/2$ and $I = 3/2$) showed that we can acquire the information both on the QI magnitude and sign. In this article, we present the temperature investigations of the EPR spectra (temperature region $T = 1.8$, 4.2, 100–400 K) and HFS signals of odd isotopes Gd^{3+} in $PbMoO_4$, $Pb_5Ge_3O_{11}$, and YVO_4.

The further consideration will touch only these materials, where the local symmetry of ICs is higher than rhombic symmetry. In this case, the HFI tensor can be represented as diagonal one with parameters $A_z = A_{\|}$, $A_x = A_y = A_{\perp}$, while the QI is determined by the only parameter P_2^0 [1]. We also note that the determination of P_2^0 is possible only with the observation of EPR transitions $M, m \longleftrightarrow M'm'$ ($\Delta S_z = \Delta M \neq 0$) with varying the projections of the nuclear spin (these are the forbidden transitions (FTs) with $\Delta I_z = \Delta m \neq 0$), the probability of which W_{fi} is usually low [1]. Magnitudes of W_{fi} increase in perpendicular orientations of external magnetic field H due to mixing nuclear states by strong QI. However, positions of FTs at $|P_2^0| < |A_{\perp}|$ are such that they are masked by the wings of intense allowed transitions (ATs) with $\Delta m = 0$, while at $|P_2^0| \geq |A_{\perp}|$, the FTs are remote from the HFS center by the magnitude ~$2P_2^0$; therefore, they are observable. Such structures are described in [2] for Gd^{3+} in YPO_4 and Ir^{2+} in MgO, CaO for the $1/2 \longleftrightarrow -1/2$ electron transition, where the relative positions of HFS components are symmetric relative to the center and are independent of the signs of parameters of the spin Hamiltonian (SH). It should be noted that without taking into account strong QI, magnitudes $A_{\perp}$ determined from the HFS, as for example in [3], are always smaller than actual ones by a factor of 1.3–1.4.

The goal of our study was to show that investigations of the HFS structure of EPR transitions of odd isotopes Gd^{3+} in different crystals at $|P_2^0| \geq |A_{\perp}|$ make it possible to determine not only the components of

tensor A but also the absolute value of P_2^0 (if the sign of b_2^0 is known) at different temperatures.

The studied single crystals with the Gd^{3+} impurity are convenient for such investigations since the EPR signals are narrow, condition $|P_2^0| > |A_i|$ is fulfilled, and magnitudes and signs of b_2^0 and P_2^0 are different. Results of this study were partially reported in [4–6].

2. EXPERIMENTAL RESULTS AND DISCUSSION

Temperature investigations of the EPR spectra for different orientations of the magnetic field were performed using a Bruker EMX plus spectrometer in a 3-cm range. The studied crystals were Czochralski-grown with impurity of 0.01 wt % $Gd_2^{157}O_3$ in the charge, excluding YVO_4, where the EPR spectrum of Gd^{3+} as the accompanying impurity was also observed.

Parameters b_n^m, which describe the EPR spectrum of even isotopes of Gd^{3+} at any temperature (the local symmetry of centers C_{3v} ($Pb_5Ge_3O_{11}$), S_4 ($PbMoO_4$), and D_{2d} (YVO_4)), were determined by the standard procedure. The root-mean-square deviation of the experimental and calculated positions of signals was minimized numerically. The accuracy in determining the absolute positions of signals ≤1 G, and that of relative ones is higher by an order of magnitude.

We used SHs (1) and (2) corresponding to the local symmetry of the ICs, which are written in coordinate systems where $\mathbf{Z} \parallel \mathbf{C}_n$ is the principal symmetry axis of the crystal, while directions $\mathbf{X}$ and $\mathbf{Y}$ in the plane $\perp\mathbf{C}_n$ corresponded to extrema of the angular dependence of EPR transitions:

$$H = 1/3b_2^0O_2^0 + 1/60(b_4^0O_4^0 + b_4^4O_4^4) + 1/1260(b_6^0O_6^0 + b_6^4O_6^4 + b_6^6O_6^6) + g\beta(HS) + SAI + 1/3P_2^0O_2^0(I) - g_n\beta_n(HI) \quad (\text{for } S_4 \text{ and } D_{2d}), \tag{1}$$

$$H = 1/3b_2^0O_2^0 + 1/60(b_4^0O_4^0 \pm b_4^3O_4^3) + 1/1260(b_6^0O_6^0 \pm b_6^3O_6^3 \pm b_6^6O_6^6) + g\beta(HS) + SAI + 1/3P_2^0O_2^0(I) - g_n\beta_n(HI) \quad (\text{for } C_{3v}). \tag{2}$$

All notations in expressions (1) and (2) are standard [1], and the double sign in (2) is associated with domain splitting [7].

Directions $\mathbf{H}$ were specified by angles Θ and φ. We observed narrows EPR signals (0.5–5.0 G) with the partially resolved HFS even at the natural content of gadolinium isotopes for all samples in extreme orientations (at Θ = 0, φ = 0 and Θ = 90°, φ = 45°).

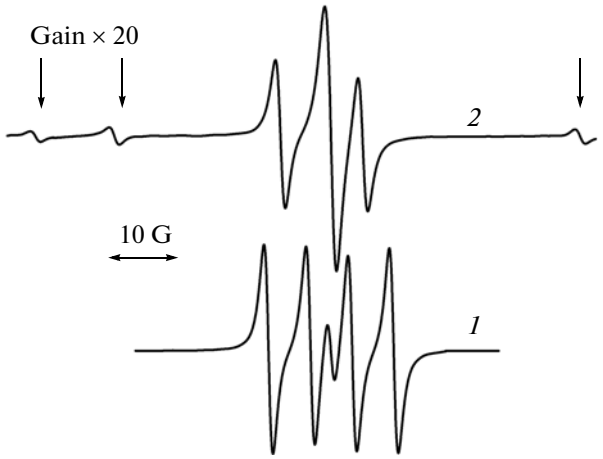

Fig. 1. Experimental HFS of EPR signals of $PbMoO_4$: Gd^{157} at $T = 100$ K in orientations (*1*) Θ = 0, φ = 0 (1/2, $m \leftrightarrow -1/2$, m); (*2*) Θ = 90°, φ = 0 (M, $m \leftrightarrow M'$, m', $M \le -1/2$, $\Delta M \approx 1$). Intense ATs with $\Delta m \approx 0$ are in the center. Arrows show transitions with $\Delta m \neq 0$.

The shape of HFS EPR signals for odd isotopes of Gd^{3+} in mentioned crystals at the microwave frequency of ~9.4 GHz and at almost all orientations of the external magnetic field excluding $\mathbf{H} \parallel \mathbf{Z}$ differs from the classical quadruple described in [1]. A clear example is presented for Gd^{157} in $PbMoO_4$ in two orientations. It is seen that at Θ = 90°, φ = 0, in addition to three intense signals with amplitude ratio 1 : 2 : 1, several weak signal lower by intensity by 2–3 orders of magnitude are observed. The HFS is asymmetric relative to H (excluding the transition 1/2, $m \leftrightarrow -1/2$, m'). For other EPR transitions, the HFS is another by shape (Fig. 2). The difference in values of splitting ΔH observed in this case (Figs. 1, 2) between intense components of transitions M, $m \leftrightarrow M'$, m with $|M| > 1/2$ ($M > M'$) varies as $|M|$ increases so that two components can merge. Such a structure is the main evidence of the fact that $|P_2^0| > |A_\perp|$. Similar HFSs of EPR transitions are also observed for our crystals.

The HFI and QI constants (we further assume that $P_2^0 = P$) of odd isotopes were evaluated using the simulation software of the HFS form for EPR transitions with well-resolved hyperfine structure for different orientations of $\mathbf{H}$. As the first step, we diagonalized the energy matrix using the complete SH ((1) and (2)) with parameters b_n^m determined for even isotopes, and seed constants for the HFI and the QI. Then, taking into account the shape of EPR lines (the Lorentzian, the Gaussian, or their mixture), the shape of the HFS of the selected EPR transition was constructed. Magnitudes of A_i, P, and the shape of lines varied until the resonant relative positions and the shape of experimental and simulated signals coincided (Fig. 2). The

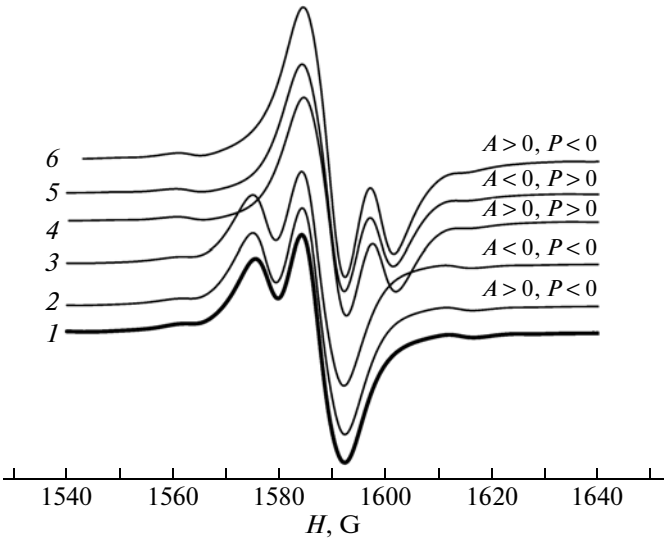

Fig. 2. (*1*) Observed HFS of the EPR signal of $PbMoO_4$: Gd^{157} at $T = 100$ K in orientation $\Theta = 90°$, $\varphi = 45°$ (M, $m \longleftrightarrow M'$, m', $M > -5/2$, $m \approx m'$, $\Delta M \approx 1$). (*2–5*) Simulated structures at different signs of A, P, and $b_2^0 < 0$, and (*6*) at $b_2^0 > 0$.

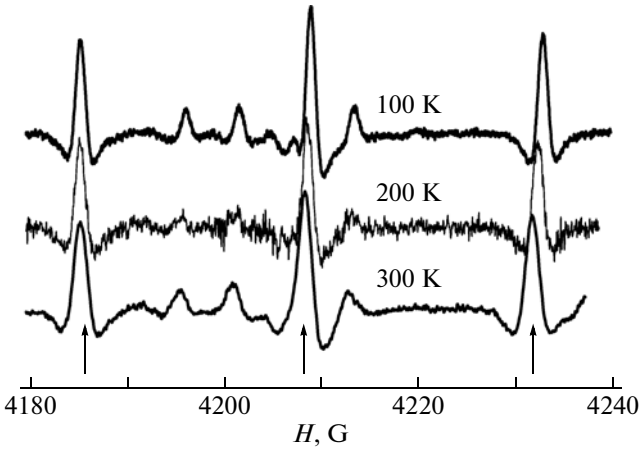

Fig. 3. Temperature variations in HFS positions of FT components 5/2, $m \longleftrightarrow 1/2$, m' ($\Theta = 0$, $\varphi = 0$, 2nd derivative) for $PbMoO_4$: Gd^{157}. Arrows show transitions with $\Delta m \approx 1$, the low-field signals are brought into coincidence on the scale H.

HFI parameters $A_\parallel$, $A_\perp$, and P were determined by relative positions of the ATs and FTs.

(i) $PbMoO_4$. Here, in addition to the ATs, the FTs, which consist of three HFS components, are observed at $\mathbf{H} \parallel \mathbf{Z}$ (Fig. 3). If magnitudes of splitting in the HFS for the ATs are almost independent of P, then ΔH for the FTs naturally also involves P. In orientations $\mathbf{H} \perp \mathbf{Z}$, magnitudes ΔH for all transitions mainly depend on $|A_\perp|$ and P.

(ii) YVO_4. The HFS of EPR signals in this crystal is resolved weakly due to the superposition of components of transitions for different isotopes. For narrowest transitions $M \longleftrightarrow M - 1$ ($|M| = 3/2, 1/2$) and $\mathbf{H} \parallel \mathbf{Z}$ and $\mathbf{H} \perp \mathbf{Z}$, edge HFS components of Gd^{155} and Gd^{157} almost merge, which leads to large errors in determining $A_\parallel$ and $A_\perp$. Although calculations predict the FT presence at $\Theta = 0$ and $\varphi = 0$, we could observe only one HFS component of possible three in our range of microwave frequencies. At $\Theta = 90°$, $\varphi = 0$, 45°, the asymmetric HFS formed both by ATs and FTs, as well as the HFS inverse by the shape, which is described for $PbMoO_4$, if we consider the EPR transitions with close M. The distinction is also in that there is always the intense signal from the even isotope.

(iii) $Pb_5Ge_3O_{11}$. In all extreme orientations, the HFS of EPR signals formed by the ATs was observed. It is asymmetric at $\Theta = 90°$, $\varphi = 0–90°$, and the FTs were observed only for a narrow and most intense transition of the $1/2 \longleftrightarrow -1/2$ types to wings of neighboring signals. Here, the resonant fields of intense signals are so that weak FTs almost always merge with them.

All found results are presented in Tables 1–3; from there, we can see that $A_\parallel \approx A_\perp$, therefore we further omit indices at A_i. We note that the data for $T = 1.8$ K are obtained from the DENR measurements [6].

In the crystals under study, almost all resolved EPR transitions were saturated at higher levels of the microwave power, especially at low temperatures. The FTs, by virtue of their low intensity, only increased by intensity in this case. During recording, amplification changed jump-likely so that FTs would be observed reliably, while the signals from ATs would not overload the spectrometer amplifier (Fig. 1).

2.1. Determination of Relative Signs of b_2^0 and P_2^0

The influence of the signs of b_2^0 and P_2^0 on the HFS shape is most clearly pronounced in the $\mathbf{H} \perp \mathbf{Z}$ orientation. To describe the features of the structure formed by ATs and FTs at $|P| \geq |A|$, let us determine the relative positions of all components for transition M, $m \longleftrightarrow M'$, m' ($M > 1/2$, and $M - M' \approx 1$). We can easily derive ΔH via solving the first-order secular equation (it is valid only for $I = 3/2$), as it was made in [2]. Omitting small terms of the type $g_n\beta_n Hm$ and $A_\perp g_n\beta_n Hm/P < 1$, we derive for energies $E(M)$

$$\begin{aligned} E(M)_{1,3} &= \Delta_{\tau c} + g\beta HM + 1/2AM \\ &\pm P \pm AM/2 \pm cM^2 \pm dM^3, \\ E(M)_{2,4} &= \Delta_{\tau c} + g\beta HM - 1/2AM \\ &\pm P \pm AM/2 \pm cM^2 \pm dM^3, \end{aligned} \quad (3)$$

Table 1. Parameters of the spin Hamiltonian for $PbMoO_4 : Gd^{157}$ (in MHz)

SH constant	Temperature, K							
	1.8	4.2	100	150	200	250	300	400
$g_{\|}$	1.9916 (9)	1.991 (6)	1.9921 (5)	1.9920 (6)	1.9920 (7)	1.9920 (6)	1.9921 (8)	1.9920 (5)
$g_{\perp}$	1.9916 (9)	1.991 (6)	1.9921 (5)	1.9920 (6)	1.9922 (7)	1.9922 (6)	1.9920 (8)	1.9920 (5)
b_2^0	−2500 (1)	−2500 (2)	−2482.6 (4)	−2464.7 (5)	−2446.6 (6)	−2429.9 (8)	−2396.1 (8)	−2361.8 (7)
b_4^0	−40.8 (3)	−40.7 (5)	−40.4 (3)	−39.8 (4)	−390.4 (2)	−38.8 (3)	−37.8 (4)	−36.8 (4)
b_6^0	0.3 (4)	0.3 (5)	0.2 (2)	0.2 (2)	0.2 (2)	0.3 (2)	0.2 (2)	0.3 (4)
b_4^4	−289 (3)	−288 (3)	−286.2 (9)	−283.7 (9)	−279.5 (8)	−277.2 (9)	−273 (1)	−266 (2)
P_2^0	−50.33 (1)	−50.3 (3)	−49.9 (3)	−49.7 (3)	−49.4 (3)	−49.2 (3)	−48.5 (3)	−47.5 (6)

Note: $A_{\|} = A_{\perp} = 16.1(3)$ MHz at all temperatures from EPR measurements, $b_6^4 \approx 7(9)$ and $b_6^6 \approx 0(5)$.

Table 2. Parameters of the spin Hamiltonian for $YVO_4 : Gd^{3+}$ (in MHz)

SH constant	Temperature, K							
	1.8	4.2	100	130	170	200	300	400
$g_{\|}$	1.9919 (7)	1.9920 (9)	1.9923 (8)	1.9915 (7)	1.9920 (9)	1.9916 (6)	1.9917 (7)	1.9920 (8)
$g_{\perp}$	1.9919 (8)	1.9920 (9)	1.9920 (6)	1.9918 (6)	1.9920 (7)	1.9916 (6)	1.9916 (8)	1.9918 (6)
b_2^0	−1438 (2)	−1437 (3)	−1419.2 (5)	−1407.3 (5)	−1389.0 (5)	−1374.1 (5)	−1322.6 (6)	−1277.1 (9)
b_4^0	−4.9 (4)	−4.9 (8)	−4.7 (3)	−4.7 (3)	−4.5 (3)	−4.6 (2)	−4.2 (1)	−4.1 (2)
b_4^4	127 (3)	127 (4)	125.8 (8)	124.6 (8)	123.8 (8)	122.8 (7)	118.7 (9)	117 (2)
P_2^0	58.65 (1)	58.6 (5)	58.0 (5)	57.6 (5)	57.1 (5)	56.6 (5)	55.1 (5)	53.4 (5)

Note: $A_{\|} = A_{\perp} = 16.2(5)$ MHz at all temperatures, $b_6^4 \approx 2(3)$ and $b_6^6 \approx 1(3)$.

Table 3. Parameters of the spin Hamiltonian for $Pb_5Ge_3O_{11} : Gd^{157}$ (in MHz)

SH constant	Temperature, K					
	1.8	4.2	100	120	200	300
$g_{\|}$	1.993 (2)	1.993 (3)	1.9918 (8)	1.9912 (8)	1.9913 (8)	1.9915 (7)
$g_{\perp}$	1.993 (2)	1.993 (2)	1.9920 (7)	1.9921 (8)	1.9922 (8)	1.9915 (8)
b_2^0	921 (3)	920 (3)	899.1 (8)	891.6 (8)	858.9 (9)	816.5 (6)
b_4^0	−123 (1)	−123 (2)	−121.1 (4)	−121.7 (4)	−120.6 (4)	−119.2 (2)
b_4^3	305 (40)	305 (50)	300 (30)	276 (45)	250 (50)	200 (30)
P_2^0	220 (3)	220 (3)	219.8 (5)	219.5 (5)	217.2 (5)	214.5 (5)

Note: $A_{\|} = 14.6(3)$ MHz, $A_{\perp} = 15.0(3)$ MHz, $b_6^3 \approx 0(20)$, and $b_6^6 \approx 0(10)$.

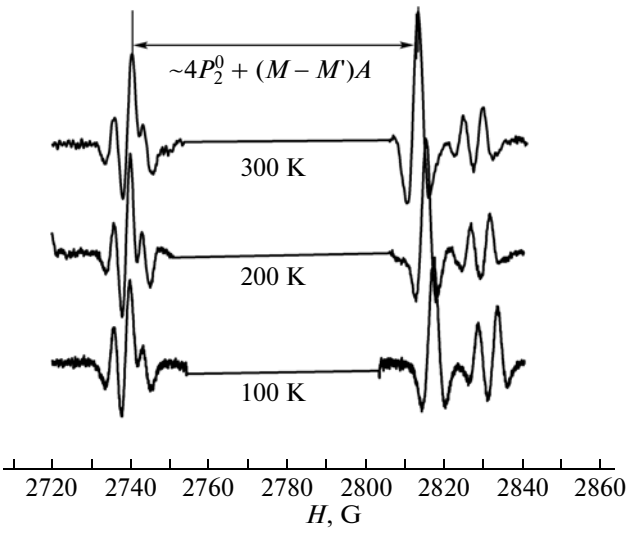

Fig. 4. Part of the HFS transition 3/2, $m \longleftrightarrow 1/2, m'$ ($\Theta = 90°$, $\varphi = 0$, 2nd derivative) in $YVO_4 : Gd^{3+}$ formed only by FTs of odd isotopes at different temperatures. Edge low-field signals are brought into coincidence on the scale H, and intense signals from even isotopes are cut.

where $c = 3A^2/8P$, $d = 3A^3/16P^2$, and $\Delta_{\tau c}$ is the contribution to E from parameters b_n^m.

For $E_{1',3'}$ and $E_{2',4'}$, expressions are similar upon the substitution of M by M'.

In this case, for ATs ($\Delta m \approx 0$ and $W_{nn'} \approx 1$, $n = n'$, $n, n' = 1–4$), we derive

$$\begin{aligned} H_{11'} &= H + c[M^2 - (M')^2] + d[M^3 - (M')^3], \\ H_{22'} &= H + A - c[M^2 - (M')^2] - d[M^3 - (M')^3], \\ H_{33'} &= H + c[M^2 - (M')^2] - d[M^3 - (M')^3], \\ H_{44'} &= H - A - c[M^2 - (M')^2] + d[M^3 - (M')^3], \end{aligned} \quad (4)$$

while for FTs ($\Delta m \neq 0$ and $W_{nn'} \approx 3A^2/16P^2$, $n' = n \pm 2$), we derive

$$\begin{aligned} H_{13'} &= H + 2P - AM' + c[M^2 + (M')^2] \\ &\quad + d[M^3 + (M')^3], \\ H_{24'} &= H + 2P + AM' + c[M^2 + (M')^2] \\ &\quad - d[M^3 + (M')^3], \\ H_{31'} &= H - 2P + AM - c[M^2 + (M')^2] \\ &\quad - d[M^3 + (M')^3], \\ H_{42'} &= H - 2P - AM - c[M^2 + (M')^2] \\ &\quad + d[M^3 + (M')^3]. \end{aligned} \quad (5)$$

It is seen from (4) that $H_{11'}$ and $H_{33'}$ are almost identical, i.e., two components merge (for example, for Gd^{157} in $PbMoO_4$, $d(M^3 - (M')^3] \approx 0.4$ G, while $|2c[M^2 - (M')^2]| \approx 1.4$ G for $M \sim 3/2$, and half-width of HFS components of transition $3/2 \longleftrightarrow 1/2 \approx 1.5$ G). $H_{22'}$ and $H_{44'}$ are remote from the center, which is determined as $H_0 = 1/2(H_{11'} + H_{33'})$, by magnitude $\sim \pm A \sim 5.7$ G. Thus, we obtained the structure consisting of three components with intensity ratio close to 1 : 2 : 1 and splitting $\sim A$. Let us determine $\Delta H_{nn'} = H_{nn'} - H_0$. It is seen from (4) that for $M > 1/2$, $\Delta H_{22'} > \Delta H_{44'}$ at any sign of A and $P < 0$ since the sign of c is determined by the sign of P ($d < c$). It follows from here that at $A > 0$, transition 44' is observed in weaker fields than 22'; consequently, the HFS is compressed from the side of smaller H since $2c[M^2 - (M')^2] < 0$. At $A < 0$ and $P < 0$, $H_{22'} < H_{44'}$, while $\Delta H_{22'} < \Delta H_{44'}$, i.e., the HFS is compressed again from the side of low fields. Thus, the HFS asymmetry is independent of the sign of A and is determined only by the signs of P, M, and M'. Absolute values of projections M, M' of the EPR transition depend on b_n^m, the signs of which are known from low-temperature investigations. Thus, the analysis of HFSs for different EPR transitions leads us to the conclusion that the observed HFS asymmetry in orientation $\mathbf{H} \perp \mathbf{Z}$ is determined by mutual signs of the largest of parameters of initial splitting (here, this is b_2^0) and P_2^0.

2.2. Temperature Dependence of SH Parameters

Variations in parameter b_n^m, the HFI, and the QI with temperature were investigated for the samples with the Gd^{3+} impurity as with the natural content of isotopes and enriched by Gd^{157}. The width of EPR signals increased as the temperature increased, especially for YVO_4. For $Pb_5Ge_3O_{11}$, all measurements were performed in the ferroelectric phase, far from the phase transition temperature, where the crystal structure reconstructs. Parameters b_n^m that we obtained coincide with the results of [8] for $PbMoO_4$ ($T = 300$ K), [9] for YVO_4 ($T = 4.2$, 298 K), and [7] for $Pb_5Ge_3O_{11}$ ($T = 100–300$ K) accurate to the measurement error.

We revealed no temperature variations in components of the HFI for our crystals, which is associated with an insufficient accuracy of experimental measurements. However, the observed anisotropy (~0.4 G) for A_i in $Pb_5Ge_3O_{11}$ can indicate that the temperature variations in components of the HFI tensor are smaller than this quantity. The magnitude of $|P_2^0|$ noticeably decreases as the temperature increases, which is seen directly from the experimental spectra (Figs. 3, 4). It follows from the data of Tables 1–3 that the b_2^0/P_2^0 ratio at mentioned temperatures is 49.7(4), –24.3(6), and 4.0(4) for Gd^{157} in $PbMoO_4$, YVO_4, and $Pb_5Ge_3O_{11}$, respectively.

The trend of the temperature dependence of b_2^0 for studied crystals, which is similar to that described for Gd^{3+} in $PbWO_4$ and $CaWO_4$ in [3, 10], can be also explained by temperature variations of lattice parameters and vibrations of lattice ions. This leads to the dependence of the crystalline-field potential A_2^0 [1, 10, 11] and gradient of the electric field of the lattice at ICs associated with A_2^0 [1]. Consequently, P_2^0 also varies. There is no data on temperature variations of A_2^0 to our knowledge. However, our results indicate that the QI varies almost proportionally to b_2^0 since ratio $b_2^0/P_2^0 \approx$ const for each of studied crystals. We previously [12] already noted to the correlation between the values of A_2^0, b_2^0, and P_2^0 for the set of different crystals with the Gd^{3+} impurity. The results of this study indicate to proportionality of two parameters of the phenomenological SH for each of selected crystals. Thus, we assume that the description of P_2^0 suggested in [12] in the context of the Newman superposition model [13] has obtained the experimental confirmation. However, we note that the seed parameters in such a model, which depend on electrostatic interactions and contributions of overlapping the electron shells of ICs and nearest anions, are possibly different not only for different by nature ligands but also for crystals. Moreover, when using the Newman model to analyze the local structure near the IC, we should take into account not only the variations in lattice parameters but the contribution to SH constants from lattice vibrations as well.

In conclusion, we can say that the EPR investigations of the HFS of odd gadolinium isotopes in different crystals under the condition $|P_2^0| > |A_\perp|$ allow us to measure the magnitude of the QI constant at different temperatures. The HFS asymmetry for perpendicular orientations of the magnetic field is determined by relative signs of P_2^0 and b_2^0 and is independent of the sign of $A_\perp$. Ratio $b_2^0/P_2^0 \approx$ const (accurate to the measurement error) at any temperature for the concrete crystal. This allows us to consider that the mechanisms forming these constants are similar to each other and to use this fact for microtheoretical calculations of SH constants.

REFERENCES

1. A. Abragam and B. Bleaney, *Electron Paramagnetic Resonance of Transition Ions* (Clarendon, Oxford, 1970; Mir, Moscow, 1972), Vol. 1; B. Bleaney, in *Hyperfine Interactions*, Ed. by A. J. Freeman and R. B. Frankel (Academic, New York, 1967; Mir, Moscow, 1970), p. 15.
2. J. C. Danner, U. Ranon, and D. N. Stamires, Phys. Rev. B: Solid State. **3**, 2141 (1971); J. Barak, A. Raizman, and J. T. Suss, J. Magn. Reson. **53**, 23 (1983).
3. S. V. Nistor, M. Stefan, E. Goovaerts, M. Nikl, and P. Bohacek, J. Phys.: Condens. Matter. **18**, 719 (2006).
4. A. D. Gorlov and D. A. Gorlov, in *Book of Abstracts of the XIV International Feofilov Symposium on Spectroscopy of Crystals Doped with Rare Earth and Transition Metal Ions, St.-Petersburg, Russia, October 18–21, 2010*, p. 66.
5. A. D. Gorlov, in *Book of Abstracts of the International Conference "Resonances in Condensed Matter," Kazan, Russia, June 21–25, 2011*, p. 23.
6. A. D. Gorlov, *Hyperfine and Super-Hyperfine Interactions* (Lambert, Saarbrücken, 2010) [in Russian].
7. V. A. Vazhenin and Yu. A. Sherstkov, Sov. Phys. Solid State **17** (8), 1655 (1975).
8. I. N. Kurkin and L. Ya. Shekun, Sov. Phys. Solid State **6** (7), 1560 (1964).
9. J. Rosental, R. F. Riley, and U. Ranon, Phys. Rev. **177**, 625 (1969).
10. J. S. M. Harvey and H. Kiefte, Can. J. Phys. **49**, 996 (1971).
11. W. M. Walsh, Jr, J. Jeener, and N. Bloembergen, Phys. Rev. A **139**, 1338 (1965).
12. L. I. Levin and A. D. Gorlov, J. Phys.: Condens. Matter. **4** (4), 1981 (1992).
13. D. J. Newman and W. Urban, Adv. Phys. **24**, 793 (1975).

Translated by N. Korovin